Journal of Power Sources 231 (2013) 97–105

Contents lists available at SciVerse ScienceDirect

Journal of Power Sources

journal homepage: www.elsevier.com/locate/jpowsour

Solid-state hydrogen storage in Hydralloy–graphite composites

Carsten Pohlmann [a], Lars Röntzsch [b,*], Felix Heubner [b], Thomas Weißgärber [b], Bernd Kieback [a,b]

[a] Institute for Materials Science, Dresden University of Technology, Helmholtzstr. 7, 01069 Dresden, Germany
[b] Fraunhofer Institute for Manufacturing Technology and Advanced Materials Branch Lab Dresden, Winterbergstr. 28, 01277 Dresden, Germany

HIGHLIGHTS

- Cyclically stable pellets of Hydralloy–graphite blends were prepared.
- Very fast (de-)hydrogenation of Hydralloy–graphite pellets are demonstrated.
- Thermal conductivity and porosity are controlled via graphite content.
- High gas permeabilities and heat conductivities in radial direction are found.

GRAPHICAL ABSTRACT

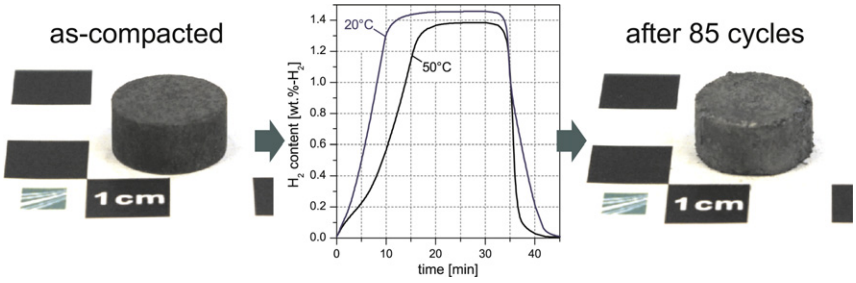

ARTICLE INFO

Article history:
Received 12 September 2012
Received in revised form
20 November 2012
Accepted 9 December 2012
Available online 20 December 2012

Keywords:
Hydrogen storage
Metal hydride
Ti–Mn–V–Fe–Zr alloy
Graphite
Thermal conductivity
Gas permeability

ABSTRACT

Hydrogen-based power systems require safe, efficient and robust hydrogen storage solutions. In this regard, metal hydrides become increasingly important because of their extremely high volumetric hydrogen capacity and their moderate operation pressures. The loading and unloading dynamics of hydride-based hydrogen tanks is mainly influenced by the intrinsic hydrogen sorption kinetics of the storage material as well as by the heat and gas transport properties of the hydride bed.

In this contribution, pelletized composites of the room-temperature hydrogen storage material Hydralloy $C5_2$ (AB_2-type) with expanded natural graphite (ENG) are discussed in view of high-dynamic hydrogen solid-state storage applications. Powdery Hydralloy $C5_2$ is blended with up to 12.5 wt.% ENG. The blend is pelletized at compaction pressures up to 600 MPa. The Hydralloy–ENG pellets exhibit an increased effective thermal conductivity and provide an increased volumetric H_2 storage capacity compared to loose powders. The hydrogenation behavior at different temperatures and for various hydrogenation–dehydrogenation cycles is discussed. Furthermore, the stability of the pellets throughout cyclic hydrogenation is evaluated. High gas permeability in radial direction and sufficient thermal conductivity in combination with a stable pellet structure underline the potential of Hydralloy–ENG composites for hydrogen storage applications with high loading dynamics.

1. Introduction

Hydrogen energy converters like fuel cells or combustion engines are strongly growing in number and often replace conventional power systems based on fossil fuels. Thus, a carbon-free energy cycle comes into sight since hydrogen can be produced via water electrolysis from renewable energy sources like wind or solar power [1,2].

Power systems based on hydrogen require safe, efficient and robust hydrogen storage solutions. In this regard, metal hydrides become increasingly important because of their extremely high volumetric hydrogen capacity and their moderate operation pressures [3,4]. Today, a large number of hydride-forming metal alloys are known [5]. Hydralloy belongs to the class of hydride-forming metal alloys (AB_2-type Ti–Mn–V–Fe–Zr alloy) which is already in commercial application, for example, for maritime fuel cells

* Corresponding author. Tel.: +49 351 2537 411; fax: +49 351 2537 399.
E-mail address: Lars.Roentzsch@ifam-dd.fraunhofer.de (L. Röntzsch).

0378-7753/$ – see front matter © 2012 Elsevier B.V. All rights reserved.
http://dx.doi.org/10.1016/j.jpowsour.2012.12.044

Notations:

ENG	expanded natural graphite
p_1	center pressure, Pa
p_2	environmental pressure, Pa
p_{eq}	equilibrium pressure, bar
R	universal gas constant, J K^{-1} mol^{-1}
T	absolute temperature, K
M	molar mass, g mol^{-1}
h	pellet height, m
r	pellet radius, m
Q	mass flow, g s^{-1}
k	gas permeability, m^2
m	mass, g
β	fitting parameter (weighing the influence of turbulences in the gas flow), m^{-1}
η	dynamic viscosity, Pa s
$\rho_{vol}^{H_2}$	volumetric hydrogen storage density, g-H_2 l^{-1}
$\rho_{grav}^{H_2}$	gravimetric hydrogen storage density, wt.%-H_2
ρ	mass density, g cm^{-3}
Φ	volume fraction, vol.%
V	volume, m^3
ΔH	enthalpy, kJ mol^{-1}
ΔS	entropy, J mol^{-1} K^{-1}

applications [6]. Hydralloy $C5_2$ has a rather low gravimetric hydrogen storage capacity of about 1.5 wt.%-H_2 combined with a high volumetric hydrogen storage capacity of about 80 g-H_2 l^{-1} [7]. Hydralloy can be classified as room-temperature hydrogen storage material because it can be hydrogenated from −20 °C to +100 °C at moderate hydrogen pressures. Moreover, it exhibits very fast intrinsic sorption kinetics [8,9]. Thus, Hydralloy is suitable for thermochemical applications, where fast responses are needed such as for non-mechanical hydrogen compressors [10,11]. A further interesting application is the usage of this material in thermochemical reactors for the continuous production of electricity with solar heat power plants, where the storage of heat at high temperature is demanded [12]. Here, a Hydralloy-based hydrogen tank can serve as the counterpart to the high-temperature hydride tank (e.g. magnesium-based) to store the hydrogen generated during day time and to release it when needed at night to rehydrogenate the high-temperature hydride [13].

The loading and unloading dynamics of hydride-based hydrogen tanks is not only influenced by the intrinsic hydrogen sorption kinetics of the storage material, but also by the heat and gas transport properties of the hydride bed. From the viewpoint of realistic hydride tank systems, the transfer of the reaction heat through the hydride bed is usually the rate-determining step, because loose powder beds are known for inferior heat transfer properties, which is a serious drawback for numerous applications [14,15]. To address this issue, materials research has studied hydride composite materials which result in increased effective thermal conductivities and which, thereby, facilitate drastically improved (un-)loading dynamics of the storage tank. According to the literature, two major routes are followed in order to realize enhanced heat conduction through the hydride bed. One route is focused on auxiliary metal structures with high thermal conductivity like nickel or aluminum fins or open-cellular foams [16–18]. Secondly, composites of hydride and graphite are being investigated [19–22]. Following this path, the thermal conductivity can be tailored very accurately. In addition, an anisotropic heat conduction behavior with strongly increased volumetric storage capacities can be realized using uniaxial compaction techniques. In our previous works [23–25] we demonstrated that pellets compacted from magnesium hydride- and complex hydride-graphite blends have superior effective thermal conductivities in radial direction, which is very beneficial considering a cylindrical geometry of the storage container. Moreover, the residual porosity can be adjusted so that the pellet fulfills the requirements of the storage compartment concerning gas permeability, mechanical stability and geometrical integrity during cycling.

In this contribution, an analogous approach is presented in order to increase the effective thermal conductivity of Hydralloy $C5_2$ as hydrogen storage material. In that respect, Hydralloy was blended with various amounts of expanded natural graphite (ENG) and compacted at different compaction pressures into cylindrical pellets. Those pellets were characterized concerning their porosities, effective thermal conductivities and gas permeabilities. From this screening, a set of parameter was chosen to produce pellets whose cyclic hydrogenation behavior was examined. Additionally, the cycled pellets were thoroughly characterized with regard to possible changes in their properties due to the hydrogenation procedure.

2. Experimental

Hydralloy $C5_2$ (51 wt.% Mn, 28 wt.% Ti, 14 wt.% V, 3 wt.% Fe, 3 wt.% Zr) was purchased from GfE Metalle und Materialien GmbH. The material was delivered in granular form in the size of 2 mm–10 mm. The granules were powderized through milling for 5 min under argon to prevent unwanted oxidation. All materials processing steps were performed under inert atmosphere following the same processing chain as described in our previous work [25]. The starting material is used in its metallic state (=dehydrogenated state) such as the magnesium-based system we previously investigated [23,24]. Thus, a comparable range of porosity and ENG volume fraction was anticipated. Therefore, the Hydralloy $C5_2$ powder was thoroughly mixed with 2.5, 5.0 and 12.5 wt.% ENG[1] (delivered by SGL Carbon) in a tubular mixer (Turbula T2F). After mixing, the Hydralloy–ENG blends were consolidated by uniaxial compaction (TIRA test 2300) at 75, 150, 300 and 600 MPa into cylindrical pellets with 14 mm in diameter whose geometric density was calculated by determining mass and volume of each pellet individually. Thereby, the residual porosity within the specimens was calculated on the basis of the theoretical density of each pellet. The theoretical density of ENG of about 2.14 g cm^{-3} was measured with a pycnometer (AccuPyc 1330). The theoretical density of Hydralloy was determined using a magnetic suspension balance (Rubotherm), where the sample weight was measured at different inert gas pressures. Due to buoyancy it is, thereby, possible to determine volume and mass of the material [26]. From that the Hydralloy density was derived which amounts to 6.1 g cm^{-3}.

In order to measure the thermal conductivity of the Hydralloy–ENG pellets, they were cut into 2 mm thin slices in axial as well as radial direction using an Accutom 5 under argon atmosphere. The specimens were examined inside a gas tight measuring cell "(cf. our previous work [25]) using the nano flash method (Netzsch LFA 447 NanoFlash) determining temperature diffusivity with an uncertainty of 3% (value given by the manufacturer). The according thermal conductivity was calculated by multiplying temperature diffusivity, density and specific heat capacity. The specific heat

[1] The contents were halved compared to the previous system [23] due to the higher theoretical density of Hydralloy of 6.1 g cm^{-3} compared to about 2.2 g cm^{-3} of $Mg_{90}Ni_{10}$.

capacity was determined using the DSC method (Netzsch DSC 204 F1 Phoenix) with an uncertainty of 3% (value given by the manufacturer).

The gas permeability in radial direction of one pellet of each parameter set was determined using a special measuring cell. For this purpose, central holes (2 mm in diameter) were drilled into the cylindrical pellets. Then, a constant flow of nitrogen is pushed through the cylindrical pellet from its center radially outwards. Thereby, the pressure in the central hole increases, which is monitored. According to the integration of the Forchheimer equation along the radius, the mass flow [Q] and the difference between the squared gas feeding pressure $[(p_1)^2]$ and the squared outside pressure $[(p_2)^2]$ fits a parabolic polynomial (cf. equation (1)) [21]. From the linear part of equation (1) the gas permeability [k] can be deduced easily:

$$p_1^2 - p_2^2 = \frac{R\cdot T}{M_{N_2}}\cdot\left[\frac{\eta}{h\cdot\pi}\cdot\ln\left(\frac{r_2}{r_1}\right)\cdot\frac{1}{k}\cdot Q + \beta\cdot\frac{1}{2\cdot\pi^2\cdot h^2}\left(\frac{1}{r_1}-\frac{1}{r_2}\right)\cdot Q^2\right] \quad (1)$$

The relative statistical error of the gas permeability has been found to amount to approximately 10%. This value has been deduced from repetitive measurements of the same pellet under equal conditions.

The hydrogenation behavior of a chosen set of pellets was examined employing thermogravimetry (TG) using a magnetic suspension balance (Rubotherm) with a precision of 10 μg. For TGA, gaseous H_2 (Linde, 99.9999% purity) was used. The pellets were placed into a clamp to simulate the geometrical constraints given in real tank. At first, all pellets were activated with four cycles at elevated temperatures up to 300 °C for about 17 h. Thereafter, up to 85 cycles were performed in a temperature range of 20–50 °C. Subsequently, the cycled pellets were characterized to examine the changes in porosity, thermal conductivity and gas permeability. Since the hydrogenated state of Hydralloy will instantly dehydrogenate at room temperature and ambient pressure, only the metallic state after cycling was characterized.

X-ray diffraction (XRD, Bruker AXS: D8 ADVANCE) using Cu Kα radiation in the angular range between 10° and 100° (2θ) was performed in the as-milled as well as in the as-cycled state. During XRD analysis, the powders were protected from ambient atmosphere using a Kapton® foil.

Furthermore, an activation process followed by 10 hydrogenation–dehydrogenation cycles was performed on smaller pellets (5 mm in diameter) in a high pressure DSC (Netzsch DSC 204 HP) coupled to a quadrupole mass analyzer (Netzsch QMS 403 C) in order to examine the chemical composition of the released gas.

All measurement errors were calculated using the law of error propagation. The total measurement errors are given by error bars in the graphs.

3. Results and discussion

3.1. Characterization of the as-compacted state

In our previous works [23–25] the as-compacted states of pellets prepared from a melt-spun magnesium alloy and two complex hydride systems with ENG were examined. It was found that the heat transfer characteristics and residual porosities can be tailored in a wide range adjusting compaction pressure and ENG content. In analogy, Hydralloy $C5_2$, as a common room-temperature hydrogen storage material, was investigated. At first, various compaction pressures and ENG contents were chosen, from which pellets are expected to cover similar ranges of thermal conductivity and residual porosity as the magnesium-based system [23]. Based on the results of that initial characterization, pellets with suitable residual porosity and heat conduction were chosen to perform hydrogenation experiments on, which are discussed in Sections 3.2 and 3.3.

Fig. 1 depicts three examples of Hydralloy–ENG pellets compacted at 300 MPa with various ENG-contents. The phase fractions and the respective errors for all processing parameters are given in Table 1. As expected from our previous works [23–25], the increase of compaction pressure and ENG-content results in a reduced residual porosity. Here, the ENG acts as a lubricant during the compaction process. Furthermore, ENG facilitates the mechanical stability of the Hydralloy–ENG pellets. Indeed, pellets made from pure Hydralloy without ENG were not mechanically stable within the considered compaction pressure range.

From the fractions of all phases involved (Hydralloy, ENG and residual porosity) it is possible to calculate the maximum volumetric as well as the gravimetric hydrogen storage densities of the pellets. The gravimetric storage capacity of hydrogenated Hydralloy (1.5 wt.%-H_2 [7]) is multiplied by its mass fraction in the pellet to retrieve the maximum gravimetric hydrogen storage density. The maximum volumetric storage density of a pellet can be calculated by multiplying the gravimetric storage capacity of the hydride by the mass density of the hydride and its volume fraction in the pellet (cf. equation (2)). These values cannot be determined by experiment. However, the volume fraction of the hydride (Φ_{hydride}) can be calculated from the volume fraction of the metal alloy in the pellet (Φ_{metal}) according to equation (3), where the hydride mass (m_{hydride}) is solved from equation (4). Thus, the volumetric storage capacity can be deduced with equation (5). Please note that this calculation only holds true as long as all volumetric expansions caused by hydrogenation consume from the residual porosity of the pellet ($V_{\mathrm{total}} = \mathrm{const.}$). In other words: The outer pellets dimensions are not to change while hydrogenation takes place.

$$\rho_{\mathrm{vol}}^{\mathrm{H_2}}(\mathrm{pellet}) = \rho_{\mathrm{grav}}^{\mathrm{H_2}}(\mathrm{hydride})\cdot\Phi_{\mathrm{hydride}}\cdot\rho_{\mathrm{hydride}} \quad (2)$$

$$\Phi_{\mathrm{hydride}} = \frac{m_{\mathrm{hydride}}}{V_{\mathrm{total}}\cdot\rho_{\mathrm{hydride}}} \quad (3)$$

$$\Phi_{\mathrm{metal}} = \frac{m_{\mathrm{metal}}}{V_{\mathrm{total}}\cdot\rho_{\mathrm{metal}}} = \frac{m_{\mathrm{hydride}}\cdot\left(1-\rho_{\mathrm{grav}}^{\mathrm{H_2}}(\mathrm{hydride})\right)}{V_{\mathrm{total}}\cdot\rho_{\mathrm{metal}}} \quad (4)$$

$$\rho_{\mathrm{vol}}^{\mathrm{H_2}}(\mathrm{pellet}) = \frac{\rho_{\mathrm{grav}}^{\mathrm{H_2}}(\mathrm{hydride})\cdot\Phi_{\mathrm{metal}}\cdot\rho_{\mathrm{metal}}}{\left(1-\rho_{\mathrm{grav}}^{\mathrm{H_2}}(\mathrm{hydride})\right)} \quad (5)$$

Fig. 2 depicts the calculated maximum volumetric and gravimetric hydrogen storage densities of all Hydralloy–ENG pellets. As expected, the increase in compaction pressure coupled with

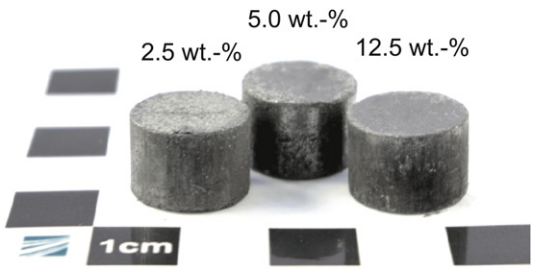

Fig. 1. Hydralloy–ENG pellets compacted at 300 MPa with an ENG-content of 2.5, 5.0 and 12.5 wt.%.

Table 1
Volume fractions of porosity, ENG and Hydralloy for all ENG weight fractions and compaction pressures.

ENG [wt.%]	Compaction pressure [MPa]	Porosity [vol.%]	ENG [vol.%]	Hydralloy [vol.%]
2.5	75	34.9 ± 2.0	4.4 ± 0.4	60.6 ± 4.0
	150	30.6 ± 2.6	4.7 ± 0.6	64.6 ± 4.9
	300	26.7 ± 2.2	5.0 ± 0.6	68.3 ± 4.1
	600	22.2 ± 3.2	5.3 ± 1.0	72.5 ± 5.7
5.0	75	31.1 ± 1.6	9.0 ± 0.6	59.9 ± 3.7
	150	25.9 ± 1.3	9.7 ± 0.7	64.4 ± 3.1
	300	22.3 ± 1.5	10.2 ± 0.9	67.6 ± 3.4
	600	19.4 ± 1.9	10.5 ± 1.3	70.1 ± 4.5
12.5	75	30.0 ± 1.7	20.3 ± 1.3	49.7 ± 6.1
	150	23.5 ± 1.9	22.2 ± 2.0	54.3 ± 7.2
	300	19.3 ± 1.5	23.4 ± 2.0	57.3 ± 6.2
	600	15.7 ± 2.0	24.4 ± 3.3	59.9 ± 8.9

a decreased porosity leads to higher volumetric storage densities. Higher ENG-contents, however, relate to lower gravimetric hydrogen storage densities, since the graphite is considered not to participate in the storage of hydrogen. The beneficial effect of compaction becomes obvious if one compares these values with the maximum volumetric storage densities of commonly used loose powders. Applying DIN EN ISO 3923 the apparent density of Hydralloy powder was determined with 1.8 g cm^{-3} which refers to 71 vol.% of porosity resulting in 27 g-H_2 l^{-1}. A loose blend of Hydralloy powder with 5 wt.% ENG achieves only 14 g-H_2 l^{-1}. In that sense, the values presented in Fig. 2 hold true only if the geometrical dimensions of the pellets are not changed during hydrogenation. Therefore, the values present possible maximum densities which are most likely to be fulfilled by pellets with high porosity so that volume changes of the storage material are compensated by the inner porosity only. The lowest porosity of 22.2 vol.% was achieved with 600 MPa compaction pressure using 2.5 wt.% ENG. Therefore, it is unlikely that the swelling of this pellet during hydrogenation can by compensated by the inner porosity only. In this study, the same geometry is needed for all pellets for the sake of comparability. Hence, a compaction pressure was chosen which results in a porosity at which no pellet swelling occurs (see Section 3.2).

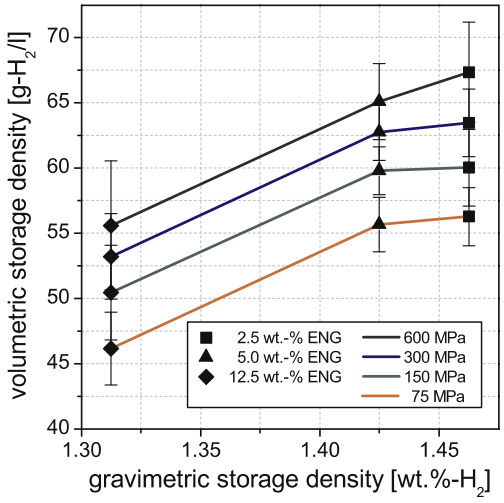

Fig. 2. Calculated maximum volumetric vs. maximum gravimetric hydrogen storage densities of Hydralloy–ENG pellets.

Nevertheless, Fig. 2 illustrates the high potential of compaction in order to increase the volumetric storage density. Pellets with the lowest volume fraction of Hydralloy (49.7 vol.%; compacted at 75 MPa with 12.5 wt.% ENG) still exceed the volumetric storage density of commonly used powder beds without any ENG and, hence, poor heat conduction properties by 150%.

The effective thermal conductivities of the Hydralloy–ENG pellets are plotted in Fig. 3a. The ENG content in the diagram is given in volume percent of the compacted composite since the effective thermal conductivity of a multi-component material is determined on the basis of the respective volume fractions. It slightly increases with increasing compaction pressure since the volume fraction of the residual porosity is decreased (cf. Table 1). As examined in our previous works [23–25] a strong anisotropy between the heat conduction perpendicular (radial) and parallel (axial) to the direction of compression can be achieved. The thermal conductivities in radial direction vary between 2.4 and 62.8 W m^{-1} K^{-1}, whereas the thermal conductivities in axial direction remain constant in the range of 2–8 W m^{-1} K^{-1}. As previously reported [25] only a minor difference in radial thermal conductivity at equal ENG contents and varying compaction pressures is examined, which indicates only an insignificant influence of the residual porosity. Fig. 3b depicts the thermal conductivities of the complex hydride systems (from our previous results) in comparison with the Hydralloy–ENG pellets. At equal ENG volume fractions similar radial thermal conductivities can be achieved independent of the primary powder used. This holds true even though the porosities at given compaction pressures vary with the storage material system. Due to a high aspect ratio (long and thin) of the magnesium flake-based material system, its effective thermal conductivity is also influenced by porosity [23]. It is, therefore, deduced that as long as powdery starting materials with low intrinsic thermal conductivities are used, the ENG content is the major control parameter to determine the effective heat conduction of suchlike pellets. Pellets of pure ENG (<5 vol.% porosity) have a radial thermal conductivity of about 370 W m^{-1} K^{-1} [23]. From that the rule of mixture is applied to illustrate the thermal conductivity versus porosity of ENG-pellets. Obviously, the measured values of the Hydralloy–ENG pellets are very close to that simple rule (cf. Fig. 3b). This indicates that the use of ENG is very effective to adjust the heat conduction inside hydride reaction beds.

The gas permeabilities of the Hydralloy–ENG pellets measured in inert atmosphere are depicted in Fig. 4. The examined gas permeabilities range from 0.6×10^{-15} m^2 to 9.7×10^{-15} m^2. As expected, the gas permeability decreases with increasing compaction pressure. Furthermore, at equal compaction pressures lower gas permeabilities with increasing ENG-content are determined (cf. inset of Fig. 4). At high compaction pressures, however, only minor differences of the gas permeabilities are observed. Porosity is the most important parameter to influence the gas permeability [27,28]. In turn, porosity is a function of the powder compressibility and the applied compaction pressure. As shown in Table 1 the porosity decreases with increasing compaction pressure as well as with increasing ENG-content. Thus, both factors determine the volume fraction of residual porosity and, thereby, the resulting gas permeability. Fig. 4 shows the relationship between the measured gas permeabilities and the according porosities. In this regard, the gas permeability is independent of the ENG content (taking the error bars into account). Indeed, the ENG-content enhances the compressibility of the Hydralloy–ENG blend which results in lower porosity at equal compaction pressures. Hence, less void space is available, which in turn causes a higher resistance to the gas flow. From preliminary computer simulations on the hydrogenation performance of suchlike Hydralloy–ENG pellets, gas

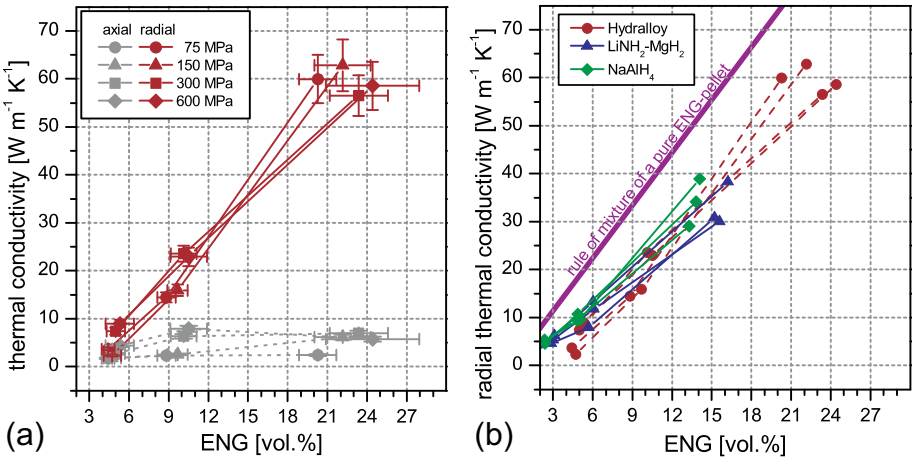

Fig. 3. (a) Thermal conductivities of the Hydralloy–ENG pellets in radial and axial direction and (b) comparison of the radial thermal conductivities of Hydralloy–ENG, sodium alanate–ENG and lithium amid–ENG pellets. Values of the complex hydride system are taken from our previous work [25].

permeabilities below 1×10^{-16} m^2 become rate-determining for the overall hydrogenation dynamics of the reaction bed. Thus, the reported values shall be sufficient to ensure fast loading and unloading of a tubular hydride reactor. The detailed simulation results based on a tubular tank with an inner diameter of 40 mm will be published elsewhere (manuscript in preparation).

3.2. Hydrogenation behavior

First hydrogenation experiments were conducted at Hydralloy–ENG pellets with an ENG content of 5 wt.% compacted at 150 MPa. The pellets expanded in axial direction by about 10%, which is due to the volume change during hydrogenation of Hydralloy. As stated in Section 3.2, a compaction pressure was chosen which results in a certain porosity, where no swelling of the pellets during hydrogenation occurs. Therefore, the compaction pressure of 75 MPa was selected in order to provide more porosity in the as-compacted state, which compensates the volume increase of the storage material. Indeed, considering a hydrogen storage tank, an optimal combination of initial porosity and pellet swelling will lead to a high volumetric storage density. Future investigations will focus on the influence of the compaction pressure on the hydrogenation properties as well as on pellet shape evolution.

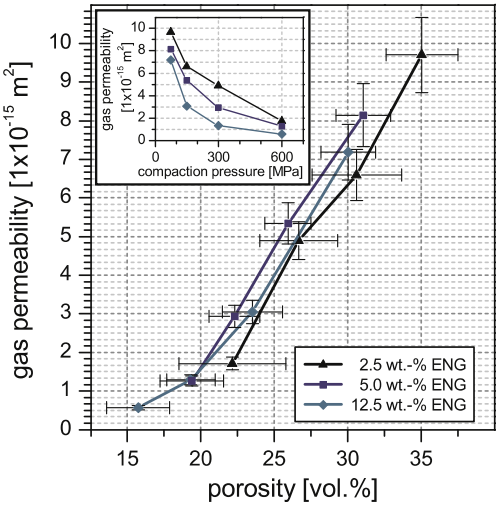

Fig. 4. Gas permeability vs. compaction pressure (inset) and gas permeability vs. porosity of the Hydralloy–ENG pellets investigated.

The pellets chosen in this study (75 MPa and 5 wt.% ENG) have an average thermal conductivity of 14.4 W m^{-1} K^{-1} and a porosity of 31.1 vol.%. The pellets were placed inside a clamp (cf. Fig. 10b) to simulate the geometrical constraints given in a real tubular tank.

Various experiments were conducted altering the number of cycles, hydrogenation and dehydrogenation pressures and temperatures. At first, an activation procedure is performed where the pellet is annealed in a hydrogen atmosphere for 17 h with temperatures at 50 °C and 300 °C and varying pressures from 0 bar to 5 bar and 0 bar to 10 bar, respectively. This is supposed to reduce any possible residual oxide layers. Within the first hydrogenation cycles an improvement of the sorption kinetics of the pellet is observed (cf. Fig. 5a). Already during the second cycle the sorption kinetics of the pellet becomes optimal. Fig. 5b depicts the hydrogenation and dehydrogenation rates of the first and the tenth cycle. The hydrogenation rate of the tenth cycle is higher than that of the first one. Furthermore, the hydrogenation is completed earlier. After the second cycle no further changes can be noticed. The high dehydrogenation kinetics are constant from the very first cycle and show a maximum dehydrogenation rate of about −0.9 wt.%-H_2 min^{-1}.

Fig. 6 presents a comparison of the first cycles after activation with different peak temperatures of 100 °C and 300 °C. After four cycles the specimen activated at 100 °C has reached its full sorption performance. However, it is not possible to dehydrogenate the pellet completely which reduces its reversible hydrogen storage density by about 0.07 wt.%-H_2.

The improvement in kinetics can be attributed to residual oxide layers not being reduced within the activation procedure, which also may explain the slower recovery after activation at 100 °C, or to hydrogen decrepitation [29]. In conclusion, it is possible to reduce the activation temperature, which, in turn, increases the number of following cycles with slower hydrogen sorption performance. Besides that a slight decrease in hydrogen storage density of the pellet has to be taken into account.

Typical (de-)hydrogenation cycles conducted at 20 °C and 50 °C are plotted in Fig. 7. The hydrogenation at 20 °C and 50 °C was carried out at hydrogen pressures of 30 bar and 40 bar, respectively. The dehydrogenation for both temperatures was performed under 1 bar hydrogen in each case. Dehydrogenation at vacuum (10^{-2} mbar) would result in an additional release of hydrogen, which is, however, not meaningful in view of practical applications. During cycling a reversible gravimetric storage density of 1.45 wt.%-

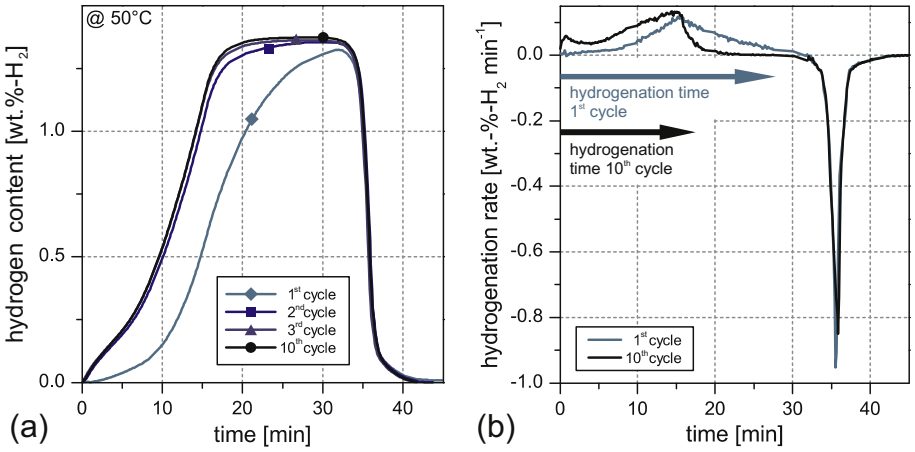

Fig. 5. (a) Comparison of the initial hydrogenation cycles (activation). (b) Hydrogen sorption rate at 40 bar and 1 bar H_2 pressure for hydrogenation and dehydrogenation, respectively.

H_2 and 1.37 wt.%-H_2 at 20 °C and 50 °C is achieved, respectively. These values refer to volumetric storage densities of the pellet of about 56 g-H_2 l^{-1} and 53 g-H_2 l^{-1} at 20 °C and 50 °C, respectively. From Fig. 2 values of about 1.43 wt.%-H_2 and 55.7 g-H_2 l^{-1} were predicted for a group of equally processed pellets which is in very good agreement with the experimental values. Slight differences can be attributed to variation in porosity of a single pellet compared to the whole group. Furthermore, due to thermodynamic changes the maximum hydrogen storage capacity increases with decreasing temperature [3]. This also influences the slopes of hydrogenation and dehydrogenation. Namely, the difference between applied pressure and equilibrium pressure, which can be considered as one part of the driving force of the reaction, is larger at 20 °C during hydrogenation. Skripnyuk et al. [8] reported an enthalpy (ΔH) of −28.7 kJ mol^{-1} and an entropy (ΔS) of −116.9 J mol^{-1} K^{-1} of Hydralloy $C5_2$, which, according to the van't Hoff equation (cf. equation (6); from Ref. [3]), results in about 10 bar and 29 bar at 20 °C and 50 °C, respectively. From that follows that pressure differences of about 20 bar and 10 bar are applied to the respective equilibrium pressures at 20 °C and 50 °C. Therefore, a faster hydrogenation is observed at 20 °C compared to 50 °C. During dehydrogenation this effect can be discussed vice versa. There, the difference between equilibrium pressure and dehydrogenation

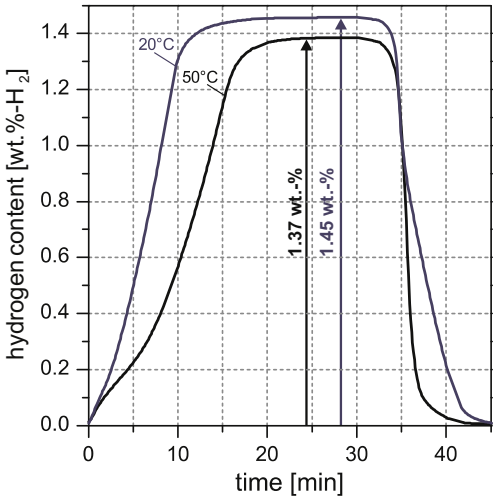

Fig. 7. Exemplary hydrogenation cycle at 20 °C and 50 °C for 1 bar H_2 back-pressure.

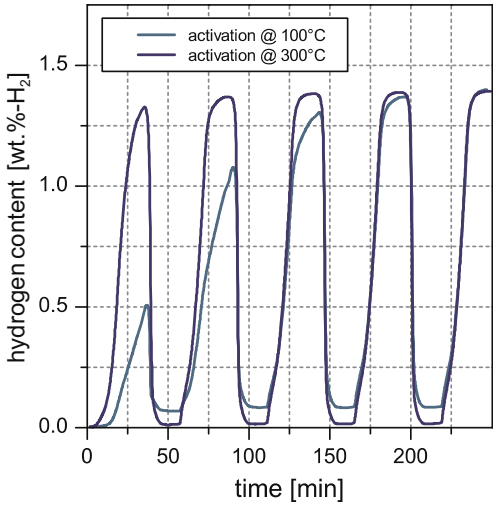

Fig. 6. Comparison of the initial cycles after activation at 100 °C and 300 °C.

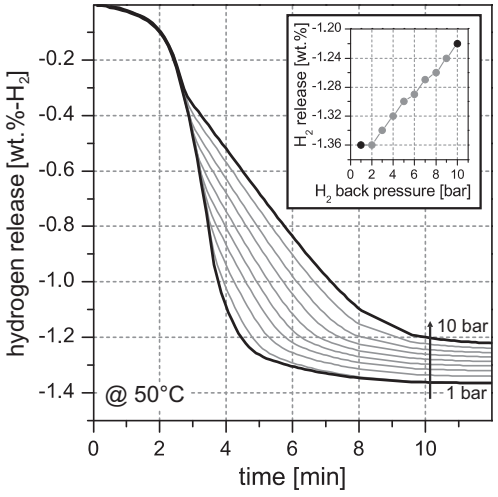

Fig. 8. Dehydrogenation against various H_2 back-pressures at 50 °C.

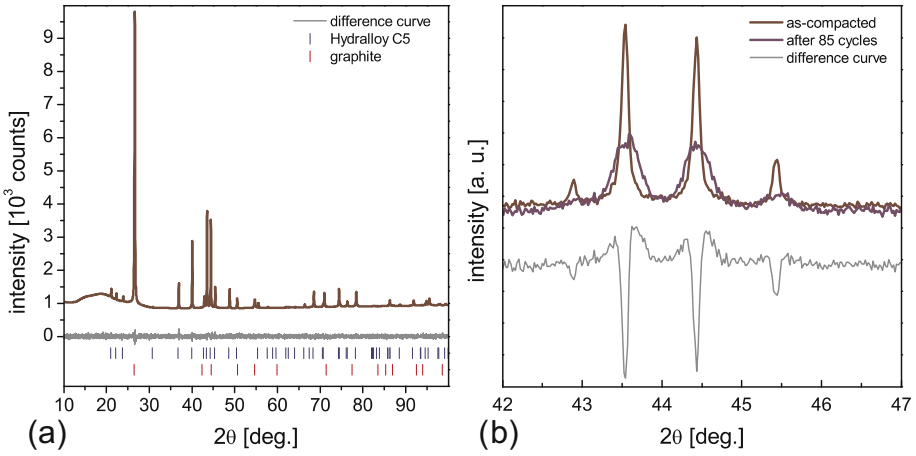

Fig. 9. X-ray diffraction patterns of Hydralloy C5 with 5 wt.% ENG (Cu Kα radiation): (a) exemplary Rietveld refinement of the as-compacted material and (b) comparison of an enlarged section of the X-ray diffraction patterns of the as-compacted state and after 85 cycles of (de-)hydrogenation.

pressure is higher at 50 °C which results in a steeper slope compared to 20 °C.

$$\ln\left(\frac{p_{eq}}{p_0}\right) = \frac{\Delta H}{R}\cdot\frac{1}{T} - \frac{\Delta S}{R} \quad (6)$$

If hydrogen conversion units like fuel cells or internal combustion engines are supplied with hydrogen from hydride storage tanks, it is inevitable to provide hydrogen at supply pressures above ambient pressure in order to avoid additional compressor stages. Thus, Hydralloy–ENG pellets have been dehydrogenated against a certain hydrogen back-pressure from 1 bar to 10 bar (cf. Fig. 8). At first, it can be noted that even at the highest back-pressure of 10 bar a fast dehydrogenation within the first 10 min can be realized. The reversible gravimetric storage density is almost linear decreasing from 1.36 wt.%-H_2 to 1.22 wt.%-H_2 with increasing back-pressure. The change in slope occurs when isobar conditions are achieved. The possibility to rapidly release hydrogen against high pressures also enables this storage material to be used in form of thermochemical hydrogen compressors. There a change between hydrogenation and dehydrogenation at different temperatures might be used to realize a compression step [10,11].

Fig. 9 depicts the X-ray diffraction patterns of Hydralloy $C5_2$ with 5 wt.% ENG. Rietveld refinement on the patterns of the as-compacted state and after 85 cycles (Hydralloy space group: $P6_3/mmc$) was performed. An exemplary refinement of the as-compacted material is given in Fig. 9a. The main results of the refinements with their statistical uncertainties are presented in Table 2. Note that the calculated phase fractions are of high uncertainty which is caused by a strong correlation of the orientation with the phase fraction in the case of graphite. The grain size determination of Hydralloy, however, is not affected by that. According to Table 2, a grain size (assuming spherical grains) of 108 nm and 15 nm was determined for the as-milled and as-cycled state, respectively. This is supported by the observed reflex broadening as depicted in the enlarged section of the XRD-patterns in Fig. 9b. During cycling with a rapid hydrogenation process (fast kinetics) many phase transformation nuclei are formed which, in turn, can result in a decrease in grain size. This also positively affects the sorption kinetics due to an increased content of grain boundaries [30]. Considering the sorption performance (cf. Fig. 5) no changes after the second cycle can be examined. However, at that point other factors could become rate-limiting which means that grain size refinement might still take place afterward. To clarify that issue in detail, XRD analyses after various numbers of cycles are necessary in future investigations.

3.3. Pellet evolution throughout cyclic hydrogenation

Table 3 lists the development of the thermal conductivities (at 20 °C and 50 °C), the gas permeabilities and the residual porosities of the Hydralloy–ENG pellets in their as-compacted and dehydrogenated states after activation and various hydrogenation/dehydrogenation cycles. Accordingly, the thermal conductivity decreased from about 14 W m^{-1} K^{-1} (14.4 W m^{-1} K^{-1} and 13.9 W m^{-1} K^{-1} at 20 °C and 50 °C, respectively) in the as-compacted state to about 7.5 W m^{-1} K^{-1} after 20 cycles and remains stable at that level even after 85 cycles. However, during activation and within the first 12 cycles it almost remained constant (around 13 W m^{-1} K^{-1}). Slight differences can be

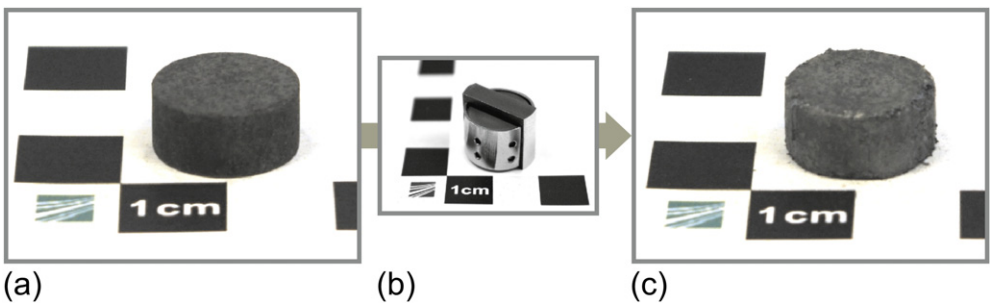

Fig. 10. Hydralloy–ENG pellets (a) in the as-compacted state, (b) inside the hydrogenation clamp and (c) in the dehydrogenated state after 85 cycles.

Table 2
Results of Rietveld refinement.

	ENG mass fraction [wt.%]	Hydralloy mass fraction [wt.%]	Hydralloy grain size [nm]
As-compacted	22 ± 12	78 ± 12	108 ± 19
After 85 cycles	27 ± 9	73 ± 9	15 ± 4

attributed to variations of single pellets. Furthermore, the carbon contents after the 12th, 20th and 80th cycle as well as in the as-compacted state according to DIN EN 9556 were determined. No significant differences were detected (5.0 wt.% ± 0.2 wt.% ENG). From these results it is assumed that during the first cycles the alternating internal expansion and contraction leads to a deterioration of contacts in the ENG network and/or a partial realignment of ENG lowering the radial thermal conductivity. In addition, particle disintegration and grain refinement can increase the overall contact resistance of heat flow [31], which also may contribute to a decrease of the effective thermal conductivity of the pellet. Nevertheless, no further changes after 20 cycles are examined and fast sorption kinetics throughout all cycles are maintained. Future investigation on larger pellets in a technically realistic test hydride tank will be performed to evaluate these issues in detail.

The gas permeability is decreased from 8.1×10^{-15} m^2 in the as-compacted state to 4.0×10^{-15} m^2 in the as-cycled state (cf. Table 3). An unexpected increase of the gas permeability after the activation procedure of 11.1×10^{-15} m^2 was measured. Pellet stability increases with cycling (cf. with next paragraph); therefore, a crack caused by the preparation procedure might be responsible for this high value. Besides this single runaway value the development stands to reason. Due to the internal volume swelling effects during hydrogen absorption and hydrogen decrepitation of the powder particles, a roughening of the surfaces and disintegration of the particle are likely to take place, which results in a higher resistance to the gas flow. In addition, a possible change in the powder particle arrangement can contribute to higher gas flow resistance. Hence, a decrease of the gas permeability is noticed. However, there is no significant difference of the gas permeability between the 40th and the 85th cycle. Thus, constant gas permeability independent of the number of cycles after some initial cycling (in analogy to the development of the thermal conductivity) can be anticipated. The lower limit of 1×10^{-16} m^2 as stated earlier is fulfilled. Thus, sufficient hydrogen flow in a tubular tank with an inner diameter of several centimeters can be assumed. Future investigations will focus on larger pellets and their hydrogenation performance in a tubular test tank.

Additionally, photographs of the as-compacted and the 85-times cycled pellet are depicted in Fig. 10. Evidently, the pellets preserve their mechanical integrity throughout cycling. Furthermore, the cylindrical shape in its initial dimensions is kept. This is underlined by the almost constant residual porosity in all states (cf. Table 3). From the mechanical processing of the pellets after hydrogenation (drilling, cutting and handling) it was found that the mechanical stability surprisingly increased compared to the initial state with increasing number of cycles. This qualitative finding may be due to the alternating swelling and shrinking during cycling which may lead to particle interdigitation which results in a stronger compact.

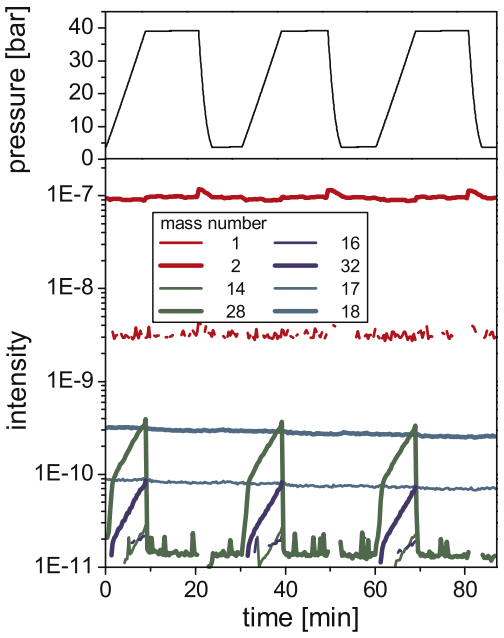

Fig. 11. Monitored mass numbers during cyclic hydrogenation with 1/**2** for hydrogen, 14/**28** for nitrogen, 16/**32** for oxygen and 17/**18** for water.

In order to rule out any unwanted chemical interaction of ENG with hydrogen during cycling, a small pellet (5 mm in diameter) was exposed to an activation process at 300 °C followed by 10 cycles at 50 °C inside a high-pressure DSC. The released gas was monitored with a quadrupole mass analyzer to scan for any gaseous C–H compounds. From the viewpoint of thermodynamics, hydrogen and carbon should form methane up to 800 K [32]. However, the atmosphere monitored throughout the whole experiment consisted of hydrogen (corresponding mass numbers: 1 and 2) and some minor residuals of oxygen (corresponding mass numbers: 16 and 32), nitrogen (corresponding mass numbers: 14 and 38) and water (corresponding mass numbers: 17 and 18). Fig. 11 depicts three exemplary hydrogenation cycles with the monitored mass numbers. During pressure build up the oxygen and nitrogen signals increase; whereas the water signal slowly decreases throughout the whole experiment. Thus, it can be assumed that the signals originate from impurities in the initial gas supply, small leakages of the gas distribution system and/or from the water contamination of the inner surfaces of the equipment, which is depleting during the experiment. No traces of any kind of C–H compounds were detected. This illustrates that Hydralloy–ENG pellets are suitable to be used in hydrogen storage applications without the formation of carbon-containing impurities in the released hydrogen.

Table 3
Evolution of thermal conductivity, gas permeability and residual porosity of the Hydralloy–ENG pellets throughout cyclic hydrogenation.

	As-compacted	After activation	After 12 cycles	After 20 cycles	After 40 cycles	After 85 cycles
λ_{rad} at 20 °C [W m^{-1} K^{-1}]	14.4	13.0	13.9	7.6	7.7	7.4
λ_{rad} at 50 °C [W m^{-1} K^{-1}]	13.9	13.0	13.4	7.4	7.6	7.4
k_{gas} [$\times 10^{-15}$ m^2]	8.1	[11.1]	–	7.0	4.0	3.9
Φ_{Por} [vol.%]	32.2	34.2	–	33.9	32.5	33.8

4. Conclusion

The feasibility of Hydralloy–ENG pellets to be used for hydrogen solid-state storage applications was demonstrated. At first, a variety of ENG-contents and compaction pressures were examined to decide on the most suitable set of parameters for cyclic hydrogenation tests. The main results are:

- Increased volumetric hydrogen storage capacities are achieved with compaction (at least 1.5 times higher than those of a loose powder bed).
- Radial thermal conductivity of the pellet can be tuned using ENG-content (up to 63 W m^{-1} K^{-1}).
- High gas permeabilities in radial direction independent of ENG-content are examined (between 0.6×10^{-15} m^2 and 9.7×10^{-15} m^2).

From these results and preliminary hydrogenation tests, pellets with 5 wt.% ENG compacted at 75 MPa were chosen for hydrogenation experiments. The major conclusions are as follows:

- After the activation process an improvement of sorption kinetics during the first few cycles was examined, which is also related to the activation temperature. Lower activation temperatures require more cycles to reach full performance.
- The grain size of Hydralloy is decreased during cyclic hydrogenation (from 108 nm to 15 nm), which is beneficial to the sorption kinetics.
- High hydrogen densities (up to 1.45 wt.%-H_2) with the possibility of fast dehydrogenation against hydrogen back pressures up to 10 bar are demonstrated.
- High geometrical stability in combination with sufficient thermal conductivity (from 14 W m^{-1} K^{-1} to 7.5 W m^{-1} K^{-1}) and gas permeability (from 8.1×10^{-15} m^2 to 4.0×10^{-15} m^2) of the pellets throughout cyclic hydrogenation was achieved.
- The formation of any gaseous C–H compounds especially during the high temperature activation procedure did not occur.

In conclusion, Hydralloy–ENG pellets have a high potential to serve as efficient and fast energy storage material for a variety of hydrogen-based power systems. The hydrogenation performance as well as the pellet evolution during the observed hydrogenation cycles is very promising to use pelletized Hydralloy–ENG composites in tubular storage tanks. Future investigations will focus on the hydrogenation behavior of those materials in a lab-scale tubular tank to confirm these findings in technical realistic environments.

Acknowledgment

This work has been performed in the framework of the European Centre for Emerging Materials and Processes Dresden (ECEMP) which is funded by the European Union and the Free State of Saxony. The authors would like to acknowledge financial support from the Fraunhofer Attract Program as well as from the BMBF (Federal Ministry of Education and Research of Germany; contract no. 03EK3020A). Furthermore, the authors would like to thank Jens Meinert for helpful discussions, Marcus Tegel for the Rietveld refinement and Thomas Hutsch for experimental support.

References

[1] C. Darras, M. Muselli, P. Poggi, C. Voyant, J.-C. Hoguet, F. Montignac, Int. J. Hydrogen Energy (2012).
[2] Enertrag, Fuel Cells Bull. 2012 (2012) 14.
[3] A. Züttel, Mater. Today 6 (2003) 24–33.
[4] G. Principi, F. Agresti, A. Maddalena, S.L. Russo, Energy 34 (2009) 2087.
[5] U. Eberle, G. Arnold, R.v. Helmolt, J. Power Sources 154 (2006) 456–460.
[6] U. Eberle, M. Felderhoff, F. Schüth, Angew. Chem., Int. Ed. 48 (2009) 6608–6630.
[7] Hydralloy Data Sheet.
[8] V.M. Skripnyuk, M. Ron, Int. J. Hydrogen Energy 28 (2003) 303–309.
[9] M.T. Hagström, P.D. Lund, J.P. Vanhanen, Int. J. Hydrogen Energy 20 (1995) 897–909.
[10] M.T. Hagström, J.P. Vanhanen, P.D. Lund, J. Alloys Compd. 269 (1998) 288–293.
[11] Z. Dehouche, N. Grimard, F. Laurencelle, J. Goyette, T.K. Bose, J. Alloys Compd. 399 (2005) 224–236.
[12] M. Felderhoff, B. Bogdanovic, Int. J. Mol. Sci. 10 (2009) 325–344.
[13] D.N. Harries, M. Paskevicius, D.A. Sheppard, T.E. Price, C.E. Buckley, IEEE Proc. 100 (2012) 539–549.
[14] D.K. Ross, Vacuum 80 (2006) 1084–1089.
[15] J. Zhang, T.S. Fisher, P.V. Ramachandran, J.P. Gore, I. Mudawar, J. Heat Transfer 127 (2005) 1391–1399.
[16] F. Laurencelle, J. Goyette, Int. J. Hydrogen Energy 32 (2007) 2957–2964.
[17] S. Mellouli, H. Dhaou, F. Askri, A. Jemni, S.B. Nasrallah, Int. J. Hydrogen Energy 34 (2009) 9393–9401.
[18] H. Wang, A.K. Prasad, S.G. Advani, Int. J. Hydrogen Energy 37 (2012) 290–298.
[19] A.R. Sánchez, H.-P. Klein, M. Groll, Int. J. Hydrogen Energy 28 (2003) 515–527.
[20] H.P. Klein, M. Groll, Int. J. Hydrogen Energy 29 (2004) 1503–1511.
[21] A. Chaise, P. de Rango, P. Marty, D. Fruchart, S. Miraglia, R. Olivès, S. Garrier, Int. J. Hydrogen Energy 34 (2009) 8589–8596.
[22] B.v. Hassel, D. Mosher, J.M. Pasini, M. Gorbounov, J. Holowczak, X. Tang, R. Brown, B. Laube, L. Pryor, Int. J. Hydrogen Energy 37 (2012) 2756–2766.
[23] C. Pohlmann, L. Röntzsch, S. Kalinichenka, T. Hutsch, B. Kieback, Int. J. Hydrogen Energy 35 (2010) 12829–12836.
[24] C. Pohlmann, L. Röntzsch, S. Kalinichenka, T. Hutsch, T. Weißgärber, B. Kieback, J. Alloys Compd. 509 (Suppl. 2) (2011) S625–S628.
[25] C. Pohlmann, L. Röntzsch, J. Hu, T. Weißgärber, B. Kieback, M. Fichtner, J. Power Sources 205 (2012) 173–179.
[26] F. Rouquerol, J. Rouquerol, K. Sing, Adsorption by Powders and Porous Solids: Principles, Methodology and Applications, Academic Press, London, 1999.
[27] A. Koponen, M. Kataja, J. Timonen, Phys. Rev. E 56 (1997) 3319–3329.
[28] N. Henderson, J.C. Brettas, W.F. Sacco, Chem. Eng. Sci. 65 (2010) 4432–4442.
[29] E.D. Koultoukis, S.S. Makridis, L. Röntzsch, E. Pavlidou, A. Ioannidou, E.S. Kikkinides, A.K. Stubos, J. Nanosci. Nanotechnol. 12 (2012) 4688–4696.
[30] M.U. Niemann, S.S. Srinivasan, A.R. Phani, A. Kumar, D.Y. Goswami, E.K. Stefanakos, J. Nanomater. 2008 (2008) 1–9.
[31] C. Uher, Thermal Conductivity of Metals, Kluwer Academic/Plenum Publishers, New York, 2005.
[32] M. Chase, J. Phys. Chem. Ref. Data (1998) 615.